Durable and Water-Floatable Ionic Polymer Actuator with Hydrophobic and Asymmetrically Laser-Scribed Reduced Graphene Oxide Paper Electrodes

Jaehwan Kim,[†] Jin-Han Jeon,[†] Hyun-Jun Kim,[†] Hyuneui Lim,[‡] and Il-Kwon Oh[†,*]

[†]Graphene Research Center, KAIST Institute for the NanoCentury, School of Mechanical, Aerospace and Systems Engineering, Division of Ocean Systems Engineering, Korea Advanced Institute of Science and Technology (KAIST), 335 Gwahak-ro, Yuseong-gu, Daejeon 305-701, South Korea and [‡]Department of Nature-Inspired Nanoconvergence Systems, Korea Institute of Machinery & Materials (KIMM), 156 Gajeongbuk-ro, Yuseong-gu, Daejeon 305-343, South Korea

ABSTRACT

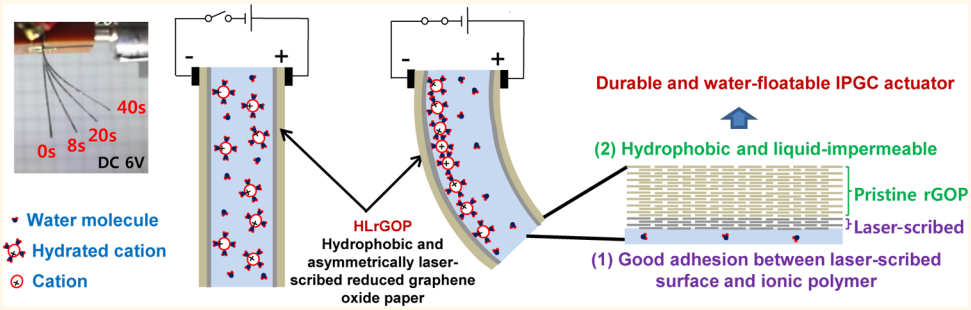

Ionic polymer actuators driven by electrical stimuli have been widely investigated for use in practical applications such as bioinspired robots, sensors, and biomedical devices. However, conventional ionic polymer—metal composite actuators have a serious drawback of poor durability under long-term actuation in open air, mainly because of the leakage of the inner electrolyte and hydrated cations through cracks in the metallic electrodes. Here, we developed a highly durable and water-floatable ionic polymer artificial muscle by employing hydrophobic and asymmetrically laser-scribed reduced graphene oxide paper electrodes (HLrGOP). The highly conductive, flexible, and cost-effective HLrGOP electrodes have asymmetrically smooth hydrophobic outer and rough inner surfaces, resulting in liquid-impermeable and water-floatable functionalities and strong bonding between an ionic polymer and the electrodes. More interestingly, the HLrGOP electrode, which has a unique functionality to prevent the leakage of the vaporized or liquid electrolyte and mobile ions during electrical stimuli, greatly contributes to an exceptionally durable ionic polymer—graphene composite actuator that is a prerequisite for practical applications in active biomedical devices, biomimetic robots, touch-feedback haptic systems, and flexible soft electronics.

KEYWORDS: laser-scribed reduced graphene oxide paper · actuator · durability · hydrophobicity · liquid permeability

Stimuli-responsive polymer actuators are smart functional materials that exhibit conformational changes under external stimuli such as changes in electric potential, pH, humidity, temperature, and light.[1−9] Materials such as electro-active polymers (EAPs) have been intensively investigated for possible use in artificial muscles, biomedical devices, bioinspired locomotive robots, rehabilitation devices for the handicapped, and micropumps.[10−13] EAPs have become an attractive emerging technology and now have a very important place in the fields of biomimetics and organic electronics because of their potential for use in various applications.

Ionic polymer metal composites (IPMCs) are a representative class of EAPs because of their outstanding capabilities like biomimetic actuation, low power consumption, high energy density, and large bending deformation under low voltage.[14,15] An IPMC

* Address correspondence to ikoh@kaist.ac.kr.

Received for review January 16, 2014 and accepted February 18, 2014.

Published online February 18, 2014
10.1021/nn500283q

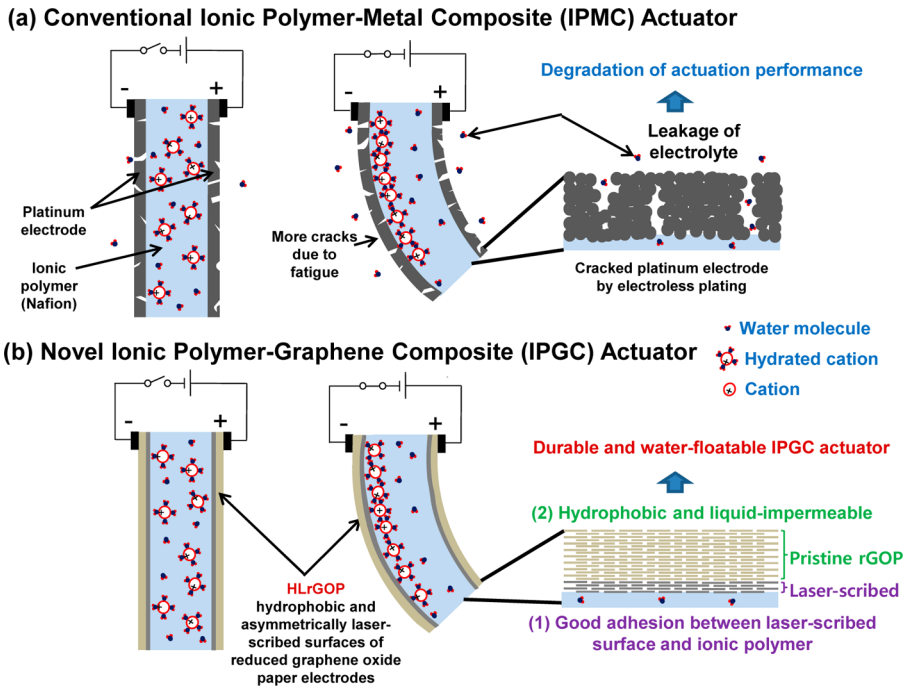

Scheme 1. Schematic representations of the structures and mechanisms of (a) liquid-permeable IPMC actuator and (b) durable and water-floatable IPGC actuator.

actuator has a "sandwich" structure that comprises an ion-exchanging polymer membrane between noble metal electrodes.[16] Among several prospective ionic polymers, Nafion, a perfluorosulfonate polymer, has been widely used in IPMC actuators because the perfluorinated polymeric structure is thermally and chemically stable. The sulfuric acid groups that are fixed in the Nafion polymer chains have a hydrophilic nature and also can absorb water molecules. In addition, the sulfuric acid groups can form ionic bonds with metallic cations such as Li^+ or Na^+ after an ion-exchange process. The hydrated cations, which bond weakly with the polar water molecules, can move through the ionic nanochannels in the Nafion under strong electric fields, resulting in bending actuation of the IPMC actuator.

Although IPMC actuators have many advantages, they are not durable under long-term excitation in open air condition due to the "mud crack" structures[16] of the metallic electrodes formed through electroless plating process, as shown in Scheme 1a and Supporting Information Figure S1. Moreover, IPMC actuators are very expensive because noble electrodes fabricated with platinum or gold must be used to protect against electrochemical oxidation. The metallic electrodes in the IPMC actuators can be deposited on an ionic polymer membrane through a very complex and time-consuming electroless plating process including sand blasting, ion absorption, primary plating, secondary plating, and ion exchange.[17] From the careful investigation of the conventional metallic electrodes, microscale mud cracks are observed on the overall electrode surface. Therefore, water molecules will evaporate, and metallic cations can leak out through the cracked metallic electrodes, resulting in reduced actuation performance for long-term actuation, as shown in Scheme 1a. Because of this critical problem, IPMC actuators with cracked metallic electrodes are not durable and their engineering applications in open air conditions will be severely restricted. In order to resolve this problem, some research groups are using ionic liquids instead of water molecules because ionic liquids provide much broader potential windows and are not fully dried in open air conditions.[15,18] However, decomposed ionic liquids under very high electric potential or leaked ionic liquids through the cracks of metallic electrodes in IPMC actuators will still cause a degradation of the actuation performance. Therefore, the use of ionic liquid for electrolyte cannot be a perfect solution to this fundamental problem related to the cracks of metallic electrodes. Nowadays, improving the durability of IPMC actuators is a major challenge in the field of artificial muscles and electroactive polymer actuators. Consequently, flexible, cost-effective, highly conductive, and crack-free electrodes that are free from the leakage of electrolyte or ionic liquids during actuation should be developed for making durable ionic polymer actuators.

For the last several years, carbonaceous papers, which are often defined as thin films made of nanomaterials such as carbon nanotubes, carbon nanofibers, and more recently, graphene, have been studied for electronic applications. Among these, graphene is of particular interest because of its one-atom-thick carbon layer with sp^2-hybridized bonds, which has

exceptional mechanical, electrical, and thermal properties.[19−21] Furthermore, graphene is promising for various applications in the domains of supercapacitors, actuators, sensors, solar cells, and biomedical devices.[22−27] In recent years, several groups have developed graphene-based actuators that respond to electrical,[28−30] electrochemical,[24,31−33] humid,[6] and infrared[34,35] stimuli. Graphene derivatives are used from simple nanofillers[28,34] in nanocomposite actuators to complex electrochemical media,[24,31−33] which induce the related reactions and volume changes by intercalation of ions on the surface and interfacial graphene layers. Furthermore, graphenes are used as simple electrodes for acoustic actuators and microactuators.[29,30] However, there are no reports of durable actuators based on functionalized reduced graphene oxide paper (rGOP) electrodes with vapor and liquid impermeability and hydrophobic properties. rGOP, which is filtered using a vacuum pump and reduced with hydroiodic (HI) acid, has high electrical conductivity, good hydrophobicity, smooth surface morphology, high flexibility, and low liquid permeability.[36−40] Additionally, it can be easily produced in large amounts because of its cost-effective formation process and facile manufacturing characteristics. However, although rGOPs can be directly used as electrodes in ionic polymer actuators, the critical problem of rGOPs is poor adhesion between electrodes and the ionic polymer. Therefore, in this study, asymmetrically modified reduced graphene oxide paper with smooth hydrophobic outer surface and laser-scribed rough inner surface (HLrGOP) was developed for use as the electrodes in durable and water-floatable ionic polymer actuators, showing good adhesion between an ionic polymer and the HLrGOPs, as shown in Scheme 1b.

Here, we report a facile synthesis method for a novel ionic polymer−graphene composite (IPGC) actuator incorporating HLrGOP electrodes with high conductivity, smooth hydrophobic outer surface, laser-scribed rough inner surface, flexibility, and cost-effectiveness. The durability of the IPGC actuator and the electrochemo-mechanical properties of the HLrGOPs themselves were investigated. The durability of the IPGC actuator is considerably enhanced compared to that of a conventional IPMC actuator in open air conditions. Furthermore, the HLrGOP offers a hydrophobic surface so that the IPGC actuator floats on water and possesses environmental robustness in humid conditions. A schematic representation comparing IPGC with IPMC and their corresponding actuation mechanisms are shown in Scheme 1b. Similar to the conventional IPMC actuator, the primary actuation mechanism of the IPGC actuator is mainly ion migration in the solid polyelectrolyte matrix rather than the quantum chemical and double-layer electrostatic effects of the HLrGOP itself. The quantum chemical and double-layer electrostatic effects are meaningful in electrolyte-filled single-walled nanotube and graphene film actuators because of dimensional changes induced by charge injection.[41,42]

RESULTS AND DISCUSSION

In order to confirm that the HLrGOP is suitable for an electrode in ionic-type artificial muscles, we first analyzed the electro-chemo-mechanical characteristics of the HLrGOP electrodes before verifying the durability performance of the IPGC actuators. The laser-scribing process of HLrGOP electrodes and the corresponding morphological investigation are shown in Figure 1. The microscale surface cracks of the platinum electrode in the IPMC actuator are shown in Figure S1. The blurred parts in Figure S1 are the ion-exchangeable polymer membranes exposed through the crack of a platinum electrode, so the inner electrolyte of the IPMC actuator can easily leak out and evaporate through the cracks in open air. However, there is no mud crack structure on the outer surface of the HLrGOP (Figure 1d). It has a very smooth surface morphology, similar to that of pure rGOP (Figure S2b), so that the leakage of electrolyte or ionic liquids in the IPGC actuator does not occur. Figure 1d shows that the laser-scribed inner surface of the HLrGOP is very rough, and the stacked rGOP is slightly expanded along the thickness direction after the laser-scribing process. This laser-scribed rough surface of the HLrGOP assists in developing a strong bond with the Nafion membrane. By properly controlling the laser power, we obtained an asymmetrically functionalized reduced graphene oxide paper electrode with mainly stacked and slightly laser-scribed layers.

Additionally, we used HI acid to reduce the GOP, as shown in Figure 1b. Compared with hydrazine (N_2H_4), HI acid as a reduction chemical is good enough to produce highly conductive rGOP electrodes.[36] This is due to the iodine doping effect during HI treatment; this effect will be described in detail in the following section on chemical analysis. As shown in Figure S2c, the thickness of pristine rGOP is 5 μm and the corresponding electrical conductivity of rGOP is 315 $S \cdot cm^{-1}$, which is acceptable for use as an actuator electrode with good flexibility, as shown in the optical image provided in Figure S2a.

Table 1 shows that the rGOP produced by HI acid reduction has the lowest sheet resistance in comparison with other graphene materials. It should be noted that GO is known as an electrically insulating material. Although the electrical conductivity of monolayer graphene mechanically cleaved by a scotch tape method is superior to the chemically produced graphene materials, it is not easy to massively produce high-quality graphene nanoflakes or to make large-scale flexible electrodes. More importantly, the sheet resistance of rGOP is much lower than those of CVD-grown graphenes.[45,47] The low sheet resistance of

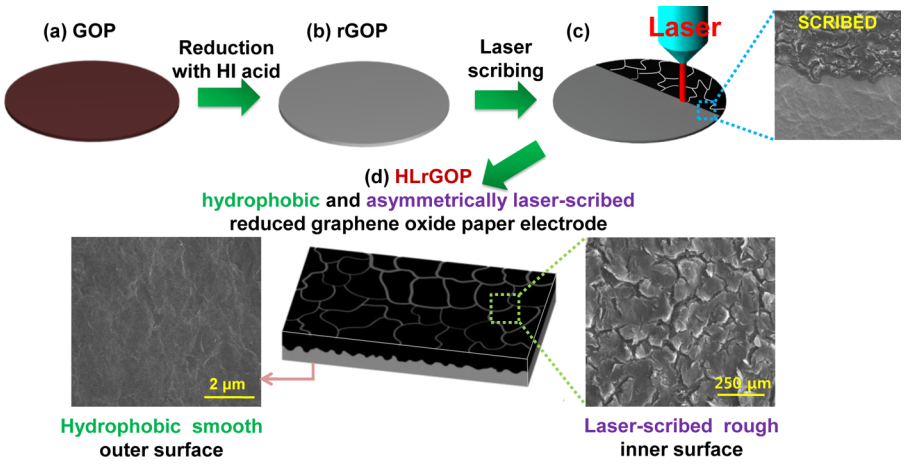

Figure 1. Synthesis of reduced graphene oxide paper electrode with hydrophobic and asymmetrically laser-scribed surfaces: (a) graphene oxide paper, (b) reduced graphene oxide paper, (c) laser scribing, and (d) HLrGOP (reduced graphene oxide paper electrode with hydrophobic and asymmetrically laser-scribed surfaces).

TABLE 1. Sheet Resistance and Electrical Conductivity of Graphene and Graphene-Derivative Materials

materials	sheet resistance (Ω/□)	thickness (μm)	conductivity (S/m)
pure graphene[43−46]	30	monolayer	~10^8
CVD-grown graphene on nickel foil[47]	280	6−10 layers	
CVD-grown graphene on glass[45]	350/2100	four layers of graphene/monolayer	
graphene oxide flake	- (insulation)	- (insulation)	- (insulation)
reduced graphene oxide flake at RT and 150 °C, respectively[48]	840000/89000	0.0007	1700/16000
reduced graphene oxide flake[49]	5000000	0.001	200
graphene oxide paper	- (insulation)	- (insulation)	- (insulation)
reduced graphene oxide paper[36]	13.89	10	7200
present reduced graphene oxide paper	**6.35**	**5**	**31500**

electrodes used in ionic-type polymer actuators is a key factor for high-performance actuation because interfacial or interlayer contact resistance between the graphene material and polymer membranes strongly affects the electric field gradient in the actuator and, consequently, its performance. Therefore, compared with other graphene and graphene derivatives, the rGOP electrode with much lower surface resistance can be a preferred material as highly conductive, flexible, and large-scale electrodes for high-performance ionic polymer actuators showing much larger bending deformations.

The chemical characteristics of the GOP, rGOP, and HLrGOP were studied using X-ray photoelectron spectroscopy and Raman spectroscopy. Figure 2a−c shows the C1s peaks of the GOP, rGOP, and HLrGOP, respectively. In the high-resolution XPS results, the C1s peaks of the rGOP and HLrGOP, compared with that of the GOP, indicate that the oxygen ratio content is reduced by HI acid reduction. Two main components, arising from C−C/C═C (284.6 eV) and C−O (~286.6 eV, epoxy and hydroxyl) groups, and two minor components, arising from C═O (~288.5 eV, carbonyl) and O−C═O (~290.4 eV, carboxyl) groups, are present on the C1s spectrum of the GOP. After reduction by HI, the C−C/C═C peak becomes dominant, whereas the signatures of the epoxy, hydroxyl, and carbonyl groups are diminished. There is a 0.6 eV binding energy shift on the C−O group, which indicates a reduction of the binding energy by the strong reducing agent. In accordance with a decrease of the oxygen content, the wettability of the GOP, rGOP, and HLrGOP, determined by the contact angles of water droplet, also changed from hydrophilic to hydrophobic. The contact angle of laser-scribed rough surface in the HLrGOP is nearly same around 89° compared with that of the smooth outer surface of rGOP. The iodine, liberated from HI during the reduction process, enhances the electrical conductivity of the rGOP and HLrGOP electrodes by doping, as shown in Figure S3.[40,50−54] The O/C ratios of the GOP, rGOP, and HLrGOP are 38.4, 10.6, and 9.8%, respectively; the I/C ratios of the rGOP and HLrGOP are 3.1 and 2.9%, respectively. The I/C ratio around 3% in both rGOP and HLrGOP is not ignorable because even a small amount of residual iodine (nearly 1% of I/C ratio) in the rGOP can greatly enhance the electrical conductivity of the rGOP.[40] Figure 2d shows the Raman spectra of the multilayered GOP, rGOP, and HLrGOP. All samples exhibit two intensity (*I*) peaks, namely, the D-band and the G-band, around 1350 and 1580 cm^{-1}. The D-band is associated with the in-plane bond-stretching motion of the C sp^2 atom pairs (the

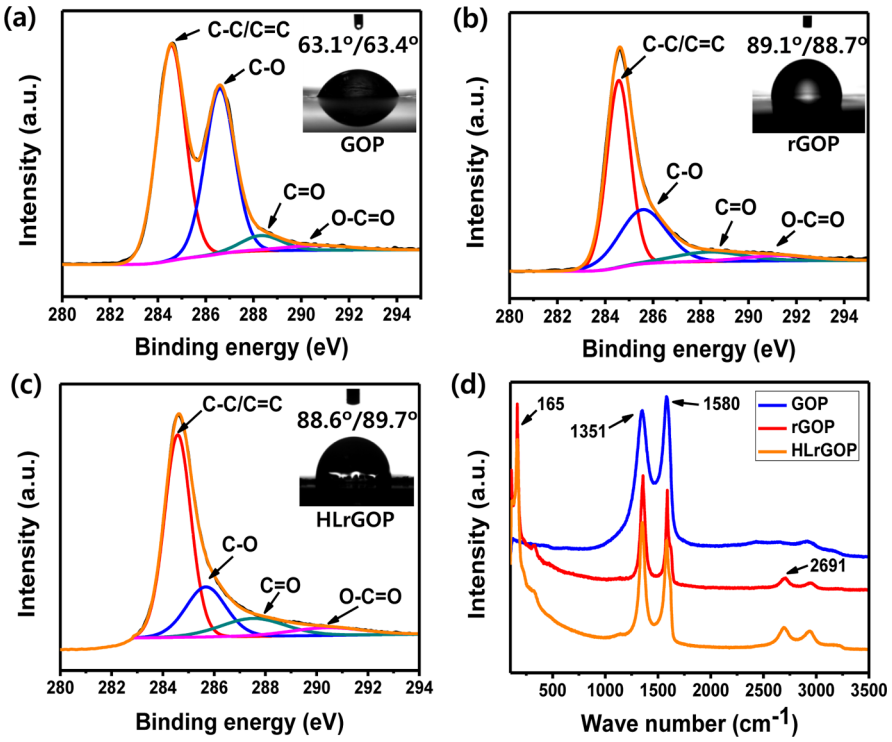

Figure 2. XPS and contact angle data showing the C1s peaks and corresponding wettabilities of (a) GOP, (b) rGOP, and (c) HLrGOP, and (d) Raman spectra of GOP, rGOP, and HLrGOP.

E_{2g} phonons) and reflects defects in the sp^2 domain. The G-band is related to the breathing modes of the rings or κ-point phonons with the A_{1g} symmetry. The I_D/I_G ratios of GOP, rGOP, HLrGOP are reported as 0.92, 1.06, and 1.14, respectively. In general, chemically reduced graphene materials show equivalent or higher I_D/I_G ratios.[50,51] Furthermore, significant 2D peaks in the rGOP and HLrGOP spectra are present around 2690 cm^{-1}. This means that the crystallinity and graphitization of the rGOP and HLrGOP are improved by reduction and laser treatment. In addition, a new peak appears at 165 cm^{-1} in the Raman spectra of rGOP and HLrGOP, known as the peak of polyiodides (I_5^-), which highly increases the electrical conductivity.[40,50−54]

With respect to the durability of the fabricated actuator, the vapor and liquid permeabilities of the electrodes are crucial. Therefore, permeability tests of GOP and rGOP electrodes for water vapor, water, and ionic liquid were conducted in this study. The water vapor permeability is measured in a glovebox, and the experimental setup is shown in Figure 3a. The glovebox maintains the amounts of H_2O and O_2 to nearly 0 in the chamber, so water can evaporate uniformly and the effects of atmospheric pollutants are diminished. The weight loss of the water by natural evaporation in the glovebox was measured. The GOP and rGOP electrodes were put on a piece of copper foil with a hole punched in it, and the edge of the paper was sealed with vacuum grease. Figure 3b shows the results of the 9 h vapor permeability experiments for GOP and rGOP samples. The measured weight losses of the water are linear under each set of conditions, and the weight-loss rates of the reference setup, GOP, and rGOP are 0.0824, 0.0476, and 0.0046 g/h, respectively. These results show that the water vapor permeability of the GOP is 10 times higher than that of the rGOP because of the capillary effect in the GO laminates.[39] The functional groups in the GOP, such as the hydroxyl, epoxy, carbonyl, and carboxyl groups, pull the water molecules toward the interior of the paper. Then, the water molecules move through the GO laminate *via* capillary effects and eventually pass through the GOP. Even though there are some defects in the rGO laminates resulting from the chemical reduction of the GO, little leakage will take place because other stacked rGO laminates prevent leakage by virtue of their hydrophobic characteristics resulting from the removal of oxygen-containing functional groups. Therefore, vaporized liquid electrolyte in the IPGC actuator can be completely protected from leakage and from the outer humid environment for a long time. To confirm the liquid impermeability of rGOP, a liquid permeability test was conducted with the experimental setup shown in Figure 3c. GOP and rGOP were placed on AAO filters and inserted between doughnut-shaped silicone membranes. After the specimen with three clamps was tightly fastened, liquid permeability tests were done with two types of liquids: water and ionic liquid (EMI-BF_4), both of which are used as electrolytes in ionic polymer actuators. Initially, the water permeation of GOP and rGOP and ionic liquid permeation of rGOP were checked at room temperature with no

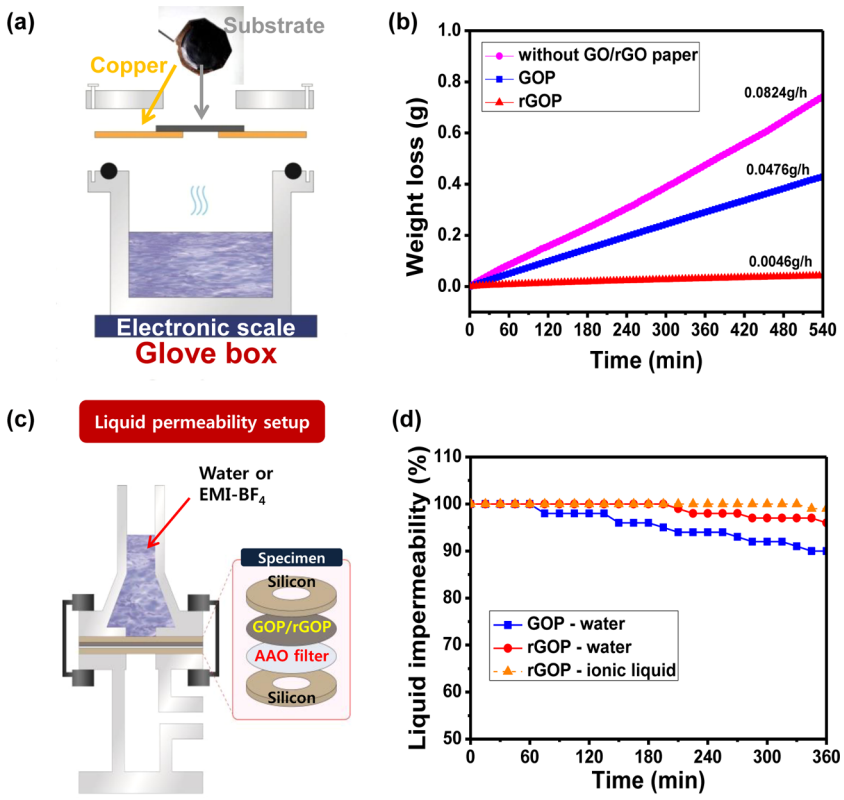

Figure 3. Vapor- and liquid-permeable tests of GOP and rGOP: (a) schematic diagram of water vapor permeability test; (b) weight loss of water vapor; (c) schematic diagram of water/ionic liquid permeability test; and (d) liquid permeability of GOP and rGOP.

external pressure or force. After 6 h, the volume of the water passing through the GOP increased to above 10% because of the capillary effects in the GO laminates. Most interestingly, the rGOP shows near impermeability for both water and ionic liquid, maintaining the volume above 96 and ≈100%, respectively, as shown in Figure 3d. Because the molecular size of ionic liquid is much larger than that of water molecules, the ionic liquid cannot easily pass through the rGOP. According to the results of vapor and liquid permeability tests, we speculate that the IPGC actuator fabricated with rGOP or HLrGOP electrodes will have exceptionally durable actuation performances because of the leakage protection of water or ionic liquid electrolytes inside ionic polymers.

During the repeatable bending actuation of the IPGC actuators, the electrical conductivity of HLrGOP electrodes was maintained due to their outstanding mechanical flexibility. In Figure 4, the electrical conductivities of rGOP and HLrGOP are plotted as a function of the cycle number of the repeatable bending test with a radius of 10 mm. Each rGOP and HLrGOP sample is tightly bonded to double-sided tape for the bending endurance experiment so that delamination does not occur during the test. The sheet resistances of rGOP and HLrGOP electrodes were measured using a probe station in real time, and the electrical conductivities were calculated using eq 1, where R_s and t are the

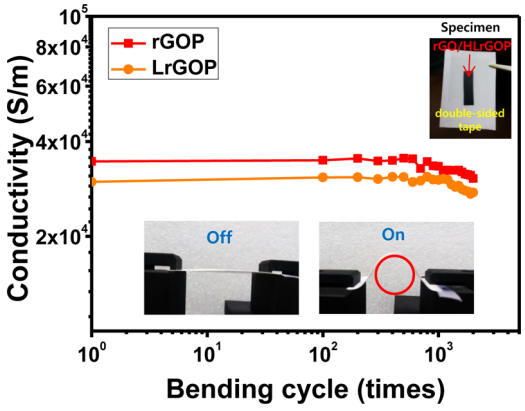

Figure 4. Electrical conductivities of rGOP and HLrGOP as a function of the number of bending cycles.

sheet resistance and thickness, respectively. The electrical conductivities of the rGOP and HLrGOP after the 2000 cycle bending test are almost the same as the initial values, resulting from their outstanding mechanical flexibility upon bending.

The rGOP and HLrGOP have better electric double-layer capacitances (EDLCs) than that of the GOP; this is because rGOP and HLrGOP have outstanding electroactive charging characteristics with the electrolyte at the interface. Since the EDLC is directly related to the performance of the ionic actuator, the cyclic voltammetric responses of electrodes should be carefully

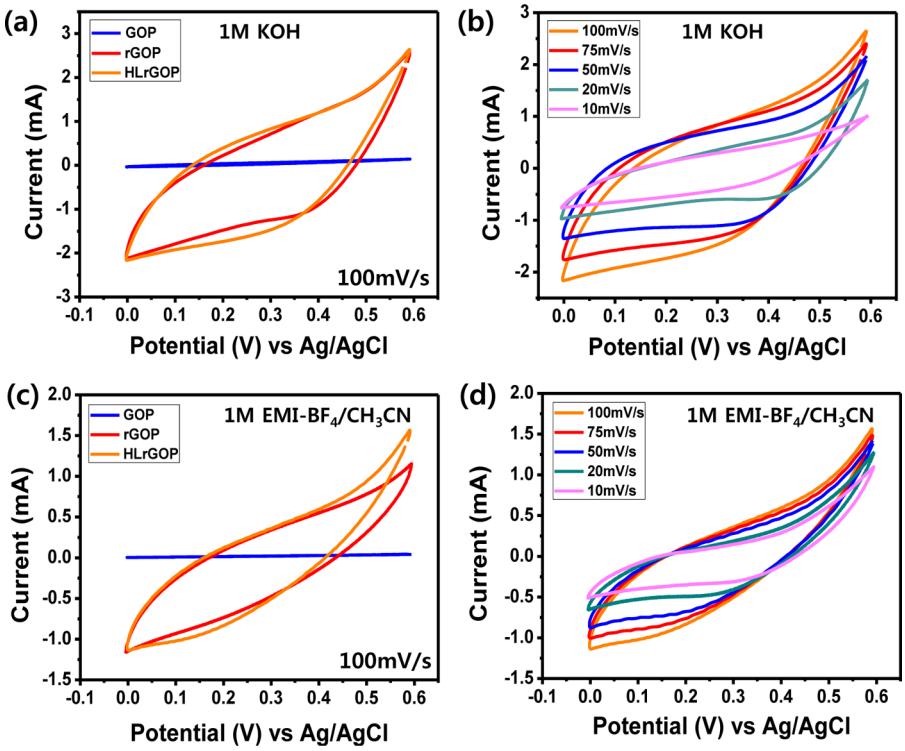

Figure 5. Cyclic voltammetry test results in 1 M KOH for (a) GOP, rGOP, and HLrGOP at a scan rate of 100 mV·s^{-1} and (b) HLrGOP at various scan rates. Cyclic voltammetry test results in 1 M EMI-BF$_4$/CH$_3$CN for (c) GOP, rGOP, and HLrGOP at a scan rate of 100 mV·s^{-1} and (d) HLrGOP at various scan rates.

TABLE 2. Specific Capacitances of GOP, rGOP, and HLrGOP in Two Different Electrolytes at Various Scan Rates

				scan rate (mV/s)				
electrolyte	specimen	potential window (V)		100	75	50	20	10
1 M KOH	GOP	0 ~ 0.6	volumetric capacitance (F/cm^3)	2.83	2.87	3.36	7.03	11.45
	rGOP	0 ~ 0.6		57.91	68.75	77.74	141.72	185.84
		−1 ~ −0.6		152.10	180.65	215.08	328.30	410.76
	HLrGOP	0 ~ 0.6		62.45	73.60	91.29	147.11	220.55
		−1 ~ 0.6		186.19	225.68	238.40	461.27	575.43
1 M EMI-BF$_4$/ acetonitrile	GOP	0 ~ 0.6		0.11	0.16	0.26	0.38	0.55
	rGOP	0 ~ 0.6		27.23	32.44	43.09	90.79	142.38
	HLrGOP	0 ~ 0.6		31.14	38.13	51.21	102.55	164.70

checked in the design of ionic polymer actuators. Figure 5a shows the cyclic voltammetric responses of the GOP, rGOP, and HLrGOP in a 1 M KOH basic solution recorded in a potential window of [0 V, +0.6 V] at a scan rate of 100 mV·s^{-1}. The volumetric capacitances of the rGOP (57.91 F·cm^{-3}) and HLrGOP (62.45 F·cm^{-3}) are superior to those of the GOP (2.83 F·cm^{-3}). Figure 5b shows the cyclic voltammetric responses of the HLrGOP at various scan rates. As the scan rate decreases from 100 to 10 mV·s^{-1}, the volumetric capacitance of the HLrGOP electrode increases. The HLrGOP shows a remarkable volumetric capacitance value of 220.55 F·cm^{-3} at 10 mV·s^{-1}, which drops to 62.45 F·cm^{-3} at 100 mV·s^{-1} in the potential window [0 V, +0.6 V]. When the potential window is changed to [−1.0 V, +0.6 V], the volumetric capacitances of HLrGOP at various scan rates have much higher values than those in the potential window of [0 V, +0.6 V], as listed in Table 2. Since a dry-type actuation test will be done with the nonaqueous ionic liquid, EMI-BF$_4$, the cyclic voltammetric responses of the GOP, rGOP, and HLrGOP in a 1 M EMI-BF$_4$/CH$_3$CN electrolyte were investigated in a potential window of [0 V, +0.6 V] at a scan rate of 100 mV·s^{-1}, as shown in Figure 5c. The volumetric capacitance values of the GOP, rGOP, and HLrGOP in nonaqueous electrolyte have a similar trend to those in aqueous electrolyte. The HLrGOP, which has the largest volumetric capacitance and the highest EDLC, is suitable for the electrodes of a high-performance ionic polymer actuator. Figure 5d shows the cyclic voltammetric curves of the HLrGOP at various scan

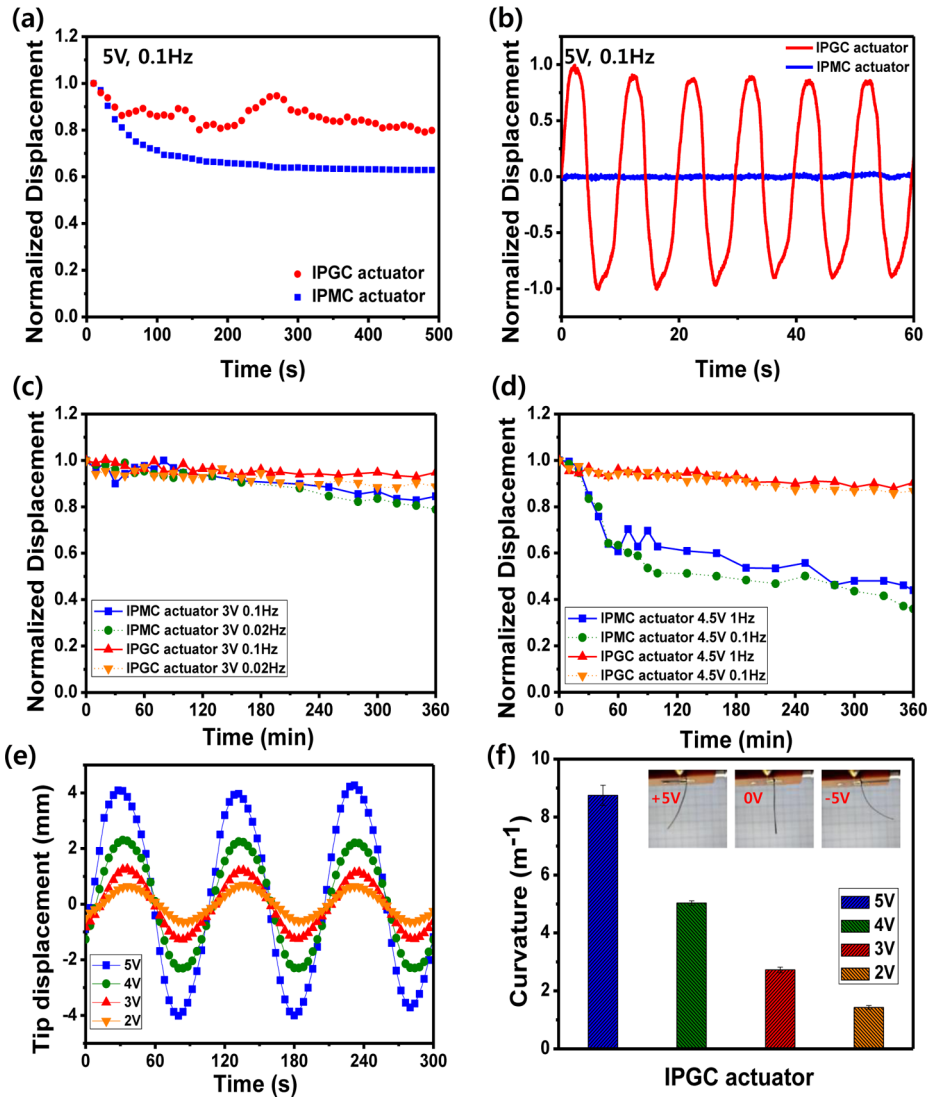

Figure 6. Open air durability test of IPGC and IPMC actuators with a water electrolyte (a) before and (b) after drying. Durability of IPGC and IPMC actuators with EMI-BF_4 electrolyte under sinusoidal electrical inputs with (c) peak voltage of 3 V and excitation frequency of 0.1 or 0.02 Hz and (d) peak voltage of 4.5 V and excitation frequency of 1 or 0.1 Hz. Bending actuation performances of IPGC actuators with EMI-BF_4 electrolyte (e) under various input voltages and (f) their corresponding curvatures.

rates. All the specific capacitances of GOP, rGOP, and HLrGOP are reported in Table 2.

As mentioned above, the laser-scribed rough surface of the HLrGOP was applied to enhance adhesion between the Nafion membrane and the electrodes; the smooth surface of unmodified rGOP often causes the delamination of the electrodes because of weak adhesion to an ionic polymer. Laser scribing increases the specific surface area of the HLrGOP and the contact area with the Nafion resin. Therefore, the HLrGOP was deposited to the Nafion membrane after brushing highly concentrated Nafion resin on the HLrGOP, as shown in Figure S4. We never observe an apparent delamination of the HLrGOP electrodes after repeatable bending tests with the flexible IPGC actuator. The wettability of the HLrGOP electrodes (contact angle ~86°) is maintained compared with the pristine rGOP (contact angle ~89°), even after hot pressing.

To confirm the durability of IPGC and IPMC actuators under extreme excitation conditions, a sinusoidal electric input with a peak voltage of 5 V and excitation frequency of 0.1 Hz was applied with water electrolyte in open air; these results are shown in Figure 6a. The IPGC actuator shows a slight degradation of the tip displacement within 20% during 500 s, while the IPMC actuator exhibits a dramatic degradation below 70% as time goes on. The performance degradation of the IPMC actuator results from the splitting of hydrogen and oxygen gas by hydrolysis at potentials over 1.23 V and from the leakage of evaporated water molecules *via* the cracked surfaces of the platinum electrodes. Water molecules in the IPGC actuator do not evaporate by virtue of the smooth surface morphology, hydrophobicity, or low permeability of the HLrGOP electrode. To more clearly demonstrate this, we dried the IPGC and IPMC actuators in an oven at 60 °C for 48 h.

TABLE 3. Weight Changes of IPGC and IPMC Actuators after Drying at 60 °C for 48 h

		condition		
actuator		before dry	after dry	after actuation
IPGC	weight (g)	0.045	0.045	0.045
IPMC		0.078	0.069	0.069

The actuation performances of the IPGC and IPMC actuators after the drying process are shown in Figure 6b. Surprisingly, the harmonic response of the IPGC actuator under a sinusoidal electrical input with peak voltage of 5 V and excitation frequency of 0.1 Hz indicates that there is no significant change in tip displacement during the experiment. The IPGC actuator after the drying process shows very durable harmonic actuation performance, similar to the actuation behavior of the IPGC actuator before drying (cf. Figure 6a). This robust response is associated with the water-impermeable properties of HLrGOP electrodes that can prevent the leakage of inner water molecules, even under extreme dry conditions. In contrast, the dried IPMC actuator does not move under electric stimulation. The total weights of IPGC and IPMC actuators before and after drying were measured to check the weight loss of water and are listed in Table 3. As anticipated by the actuation results, there is no change in the weight of the IPGC actuator before and after drying, while the weight of the IPMC actuator is reduced by 0.009 g due to the weight loss of water leaked through the cracked metallic electrode during the drying process.

Recently, ionic liquids have been used to make "dry-type" ionic polymer actuators. We measured the long-term durability of IPMC and IPGC actuators with ionic liquid electrolyte, which does not evaporate at room temperature. We selected 1-ethyl-3-methylimidazolium tetrafluoroborate (EMI-BF_4) as the inner liquid electrolyte in the ionic polymer matrix because of its high ionic conductivity, low viscosity, and good thermal and chemical stabilities. The IPGC actuators with this electrolyte show no performance degradation over an experimental period of 6 h under harmonic input with a peak voltage of 3 V and excitation frequencies of 0.1 and 0.02 Hz. The IPGC actuator outperforms the IPMC actuator, as shown in Figure 6c. The normalized tip displacement of both actuators shows robust performance for 2 h; afterward, the actuation performance of the conventional IPMC actuator gradually decreases as time proceeds. To show the dramatic difference in durability between the IPGC and IPMC actuators, we increased the applied voltage to 4.5 V that can decompose ionic liquids. However, in this condition, the IPGC actuators maintain their outstanding durability, holding their actuation performance for 6 h without an apparent drop in durability for both two different input frequencies of 1.0 and 0.1 Hz. On the other hand, the IPMC actuators are not durable over time under the same conditions, as can be seen in Figure 6d. Their normalized tip displacements rapidly decrease after 1 h, and eventually, they drop below 50% after 6 h. This rapid and large-scale degradation in durability is attributed to the loss of ionic liquid due to electrolysis at 4.5 V and the decreased electrical conductivity resulting from the growth of surface cracks by repeated large bending deformations. The EMI-BF_4 can be decomposed by the electrolysis process at an electric input voltage of 4.5 V, and decomposed ionic liquid can leak out or evaporate through surface cracks in the platinum electrodes of the IPMC actuators. Therefore, the leakage of decomposed ionic liquids degrades the actuation performance of IPMC actuators under long-term excitation. However, the IPGC actuators can remain durable at 4.5 V and maintain their normalized tip displacement above 90% after 6 h because the HLrGOP electrodes are vapor- and liquid-impermeable and hydrophobic. We also analyzed not only the durability but also the bending performance of the IPGC actuators. Figure 6e shows the harmonic responses of the IPGC actuators under four different driving voltages (2−5 V) at an excitation frequency of 0.01 Hz. As the driving voltage increases, the tip displacement of the IPGC actuator increases monotonically. The maximum tip displacement of the IPGC actuator reaches 4.26, 2.30, 1.26, and 0.69 mm under the input voltages of 5, 4, 3, and 2 V, respectively. By using eq 2, the bending curvatures κ were calculated as shown in Figure 6f. We find κ = 8.75, 5.03, 2.72, and 1.43 m^{-1} under the input voltages of 5, 4, 3, and 2 V, respectively. The inset photograph of Figure 6f shows images of the bending IPGC actuators under the sinusoidal input voltage of 5 V with an excitation frequency of 0.0025 Hz. No conventional IPMC actuator with cracked metallic electrodes can be actuated sustainably in air. In contrast, the present IPGC actuator with water or ionic liquid electrolytes shows exceptionally durable and stable actuation performances. In addition, Figure S5 shows the deformed shapes of the IPGC actuator under the step input with DC 6 V after the indicated intervals. A large bending deformation of the IPGC actuator at high driving voltage was achieved, as shown in Figure S5.

In particular, the IPGC actuator can float on the water surface by virtue of the hydrophobic HLrGOP electrodes. On the other hand, the IPMC actuator sinks, as shown in Figure S6. Additionally, in order to obtain rGOP surfaces with even greater hydrophobicity, plasma treatment with CF_4 was performed on the surface of pristine rGOP. Figure S7a shows the C1s peak of FrGOP obtained using XPS. Several peaks, such as those associated with C−C/C═C (284.6 eV), C−O (286 eV), C═O (288.4 eV), and O−C═O (290.5 eV), are present, and three more peaks related to fluorine also appear. Covalent C−F bonding is indicated at 287.2 eV, and

perfluorinated peaks related to C−F_2 and C−F_3 are present at 289.5 and 291.5 eV, respectively. The contact angle of the FrGOP surface was measured and found to reach a value of 125.2°; this is an increase of 30° from the contact angle of the pure rGOP surface. The conductivity of the FrGOP is maintained in the range of 275−315 S/cm. Figure S7b shows the F1s peak and its decomposition into three separate peaks of the FrGOP. The contact angle of the IPGC actuator after plasma treatments reaches 121°, as shown in Figure S7d. Taken together, these results indicate that a special surface treatment for higher energy surfaces using plasma technology can be used to modify and enhance the surface characteristics of these actuators in the future.

CONCLUSION

In summary, we have developed an exceptionally durable and water-floatable ionic polymer−graphene actuator (IPGC) integrated with hydrophobic and asymmetrically laser-scribed reduced graphene oxide paper electrodes (HLrGOP). The durability problem, which was the main drawback in the conventional ionic polymer−metal composite (IPMC) actuators, was resolved by utilizing liquid-impermeable, hydrophobic, highly flexible, and conductive HLrGOP electrodes. Unlike metallic electrodes deposited with electroless plating in conventional IPMC actuators, the HLrGOP electrode has a smooth outer surface morphology without apparent cracks along the thickness direction and is nearly liquid-impermeable. Also, the laser-scribed rough surface of the HLrGOP is sufficient for strong adhesion between an ionic polymer and HLrGOPs without reduction of electrical conductivity. The synthesized IPGC actuators with both water and ionic liquid electrolytes show exceptionally durable actuation without apparent degradation, even under very high input voltage of 4.5 V over 6 h. The newly designed HLrGOP electrode, which has a unique functionality to prevent the leakage of the vaporized or liquid electrolyte and mobile ions during electrical stimuli, greatly contributes to an exceptionally durable and water-floatable IPGC actuator that can be used in active biomedical devices, biomimetic robots, touch-feedback haptic systems, and flexible soft electronics.

MATERIALS AND METHODS

Preparation of HLrGOPs. Graphite oxide was prepared from natural graphite powder (Samjung C&G) using the modified Hummers method.[55] One gram of graphite was mixed with 18 mL of H_2SO_4 and 1 g of $NaNO_3$ and stirred for 5 h. Then, 3 g of $KMnO_4$ was slowly added to the mixture in an ice bath. After 6 h, 100 mL of 10% H_2O_2 was added to the mixture, and it became dark yellow. Finally, this dark yellow mixture was washed with 100 mL of 10% HCl and a sufficient amount of deionized (DI) water. This graphite oxide suspension was ultrasonicated in a homogenizer for 2 h to exfoliate the graphene oxide (GO). Graphene oxide paper (GOP) was easily fabricated by vacuum filtration of 6 mL of GO suspension through an anodic aluminum oxide (AAO) filter with a 0.02 μm pore size. The reduction process proceeded by floating the GOP on an HI acid solution at 100 °C in an oil bath for 1 h.[40] After the reduction process, the rGOP was washed with ethanol and dried in an oven for a short time. Laser scribing was done on one entire side of the rGOP at a current of 2 mA.[56]

Fabrication of IPGC and IPMC Actuators. To prepare the IPGC actuators, two Nafion-117 samples as an ionic polymer were first immersed in water and EMI-BF_4 (ionic liquid). A highly concentrated Nafion resin was brushed on the laser-scribed side of the HLrGOPs for better adhesion. The IPGC actuators were fabricated using the hot-pressing method of attaching HLrGOPs and Nafion-117 at 0.5 MPa and 80 °C for 2 min. Just like the IPGC actuators, the two Nafion-117 samples were also immersed in water and EMI-BF_4 for the preparation of the IPMC actuators. The IPMC actuators were fabricated *via* the electroless plating of platinum on the Nafion-117.[17]

Characterization. The morphology of the HLrGOPs was examined using scanning electron microscopy (SEM, Magellan400). High-resolution X-ray photoelectron spectroscopy (XPS) results were determined using an ESCA Multilab 200 system. The contact angle was measured with a Kyowa DM-501. Raman spectra were obtained with an ARAMIS. The sheet resistances of the rGOP and HLrGOP were measured with a probe station (MS TECH, model 4000). Cyclic voltammetry analyses of GOP, rGOP, and HLrGOP were done with a multichannel potentiostat/galvanostat (VersaStat, Princeton Applied Research). Measurement of the actuation performance of the IPGC and the IPMC actuators was performed using a CCD camera (XC-HR50) and a laser displacement sensor (Keyence, LK-031). A current amplifier (UPM1504) and a NI-PXI data acquisition system (NI-PXI 1042Q, PXI 6252 board) were used to generate signals and to activate the actuators.

The electrical conductivity was determined by the following equation:

$$\text{electricalconductivity}(S/m) = \frac{1}{R_s \cdot t} \quad (1)$$

where R_s and t are the sheet resistance and thickness, respectively.

The bending curvature κ was calculated by the following equation:

$$\kappa = \frac{1}{R} = \frac{2\delta}{(l^2 + \delta^2)} \quad (2)$$

where R, δ, and l are the radius of curvature, the tip displacement, and the free length of the actuator, respectively.

Conflict of Interest: The authors declare no competing financial interest.

Acknowledgment. This work was supported by a National Research Foundation of Korea Grant funded by the Korean Government (No. 2008-005994) and 2012R1A2A2A01047543.

Supporting Information Available: SEM images of rGOP, IPMC, and IPGC actuator, and the potential application to a biomimetic water strider robot, as well as the XPS and wettability of fluorinated graphene paper. The actuation performance of the IPGC actuator under DC voltage is also shown. This material is available free of charge *via* the Internet at http://pubs.acs.org.

REFERENCES AND NOTES

1. Mukai, K.; Asaka, K.; Sugino, T.; Kiyohara, K.; Takeuchi, I.; Terasawa, N.; Futaba, D. N.; Hata, K.; Fukushima, T.; Aida, T. Highly Conductive Sheets from Millimeter-Long Single-Walled Carbon Nanotubes and Ionic Liquids: Application

to Fast-Moving, Low-Voltage Electromechanical Actuators Operable in Air. *Adv. Mater.* **2009**, *21*, 1582–1585.
2. Chen, L.; Liu, C.; Liu, K.; Meng, C.; Hu, C.; Wang, J.; Fan, S. High-Performance, Low-Voltage, and Easy-Operable Bending Actuator Based on Aligned Carbon Nanotube/Polymer Composites. *ACS Nano* **2011**, *5*, 1588–1593.
3. Liang, J.; Huang, L.; Li, N.; Huang, Y.; Wu, Y.; Fang, S.; Oh, J.; Kozlov, M.; Ma, Y.; Li, F.; *et al.* Electromechanical Actuator with Controllable Motion, Fast Response Rate, and High-Frequency Resonance Based on Graphene and Polydiacetylene. *ACS Nano* **2012**, *6*, 4508–4519.
4. Richter, A.; Bund, A.; Keller, M.; Arndt, K.-F. Characterization of a Microgravimetric Sensor Based on pH Sensitive Hydrogels. *Sens. Actuators, B* **2004**, *99*, 579–585.
5. Okuzaki, H.; Kuwabara, T.; Funasaka, K.; Saido, T. Humidity-Sensitive Polypyrrole Films for Electro-active Polymer Actuators. *Adv. Funct. Mater.* **2013**, *23*, 4400–4407.
6. Park, S.; An, J.; Suk, J. W.; Ruoff, R. S. Graphene-Based Actuators. *Small* **2010**, *6*, 210–212.
7. Lendlein, A.; Jiang, H.; Jünger, O.; Langer, R. Light-Indcued Shape-Memory Polymers. *Nature* **2005**, *434*, 879–882.
8. van der Linden, H.; Olthuis, W.; Bergveld, P. An Efficient Method for the Fabrication of Temperature-Sensitive Hydrogel Microactuators. *Lab Chip* **2004**, *4*, 619–624.
9. Sánchez-Ferrer, A.; Merekalov, A.; Finkelmann, H. Opto-Mechanical Effect in Photoactive Nematic Side-Chain Liquid-Crystalline Elastomers. *Macromol. Rapid Commun.* **2011**, *32*, 671–678.
10. Rajagopalan, M.; Oh, I. K. Fullerenol-Based Electroactive Artificial Muscles Utilizing Biocompatible Polyetherimide. *ACS Nano* **2011**, *5*, 2248–2256.
11. Smela, E. Conjugated Polymer Actuators for Biomedical Applications. *Adv. Mater.* **2003**, *15*, 481–494.
12. Yeom, S. W.; Oh, I. K. A Biomimetic Jellyfish Robot Based on Ionic Polymer Metal Composite Actuators. *Smart Mater. Struct.* **2009**, *18*, 085002.
13. Fukuda, K.; Sekitani, T.; Zschieschang, U.; Klauk, H.; Kuribara, K.; Yokota, T.; Sugino, T.; Asaka, K.; Ikeda, M.; Kuwabara, H.; *et al.* A 4 V Operation, Flexible Braille Display Using Organic Transistors, Carbon Nanotube Actuators, and Organic Static Random-Access Memory. *Adv. Funct. Mater.* **2011**, *21*, 4019–4027.
14. Lu, J.; Kim, S.-G.; Lee, S.; Oh, I.-K. A Biomimetic Actuator Based on an Ionic Networking Membrane of Poly(strene-*alt*-maleimide)-Incorporated Poly(vinylidene fluoride). *Adv. Funct. Mater.* **2008**, *18*, 1290–1298.
15. Li, J.; Ma, W.; Song, L.; Niu, Z.; Cai, L.; Zeng, Q.; Zhang, X.; Dong, H.; Zhao, D.; Zhou, W.; *et al.* Superfast-Response and Ultrahigh-Power-Density Electromechanical Actuators Based on Hierarchal Carbon Nanotube Electrodes and Chitosan. *Nano Lett.* **2011**, *11*, 4636–4641.
16. Shahinpoor, M.; Kim, K. J. Ionic Polymer-Metal Composites: I. Fundamentals. *Smart Mater. Struct.* **2001**, *10*, 819.
17. Kim, K. J.; Shahinpoor, M. Ionic Polymer−Metal Composites: II. Manufacturing Techniques. *Smart Mater. Struct.* **2003**, *12*, 65.
18. Torop, J.; Palmre, V.; Arulepp, M.; Sugino, T.; Asaka, K.; Aabloo, A. Flexible Supercapacitor-like Actuator with Carbide-Derived Carbon Electrodes. *Carbon* **2011**, *49*, 3113–3119.
19. Geim, A. K.; Novoselov, K. S. The Rise of Graphene. *Nat. Mater.* **2007**, *6*, 183–191.
20. Lee, C.; Wei, X.; Kysar, J. W.; Hone, J. Measurement of the Elastic Properties and Intrinsic Strength of Monolayer Graphene. *Science* **2008**, *321*, 385–388.
21. Balandin, A. A.; Ghosh, S.; Bao, W.; Calizo, I.; Teweldebrhan, D.; Miao, F.; Lau, C. N. Superior Thermal Conductivity of Single-Layer Graphene. *Nano Lett.* **2008**, *8*, 902–907.
22. Liu, C.; Yu, Z.; Neff, D.; Zhamu, A.; Jang, B. Z. Graphene-Based Supercapacitor with an Ultrahigh Energy Density. *Nano Lett.* **2010**, *10*, 4863–4868.
23. Sridhar, V.; Kim, H.-J.; Jung, J.-H.; Lee, C.; Park, S.; Oh, I.-K. Defect-Engineered Three-Dimensional Graphene−Nanotube−Palladium Nanostructures with Ultrahigh Capacitance. *ACS Nano* **2012**, *6*, 10562–10570.
24. Xie, X.; Qu, L.; Zhou, C.; Li, Y.; Zhu, J.; Bai, H.; Shi, G.; Dai, L. An Asymmetrically Surface-Modified Graphene Film Electrochemical Actuator. *ACS Nano* **2010**, *4*, 6050–6054.
25. Wang, Y.; Yang, R.; Shi, Z.; Zhang, L.; Shi, D.; Wang, E.; Zhang, G. Super-elastic Graphene Ripples for Flexible Strain Sensors. *ACS Nano* **2011**, *5*, 3645–3650.
26. Wang, X.; Zhi, L.; Mullen, K. Transparent, Conductive Graphene Electrodes for Dye-Sensitized Solar Cells. *Nano Lett.* **2008**, *8*, 323–327.
27. Sun, X.; Liu, Z.; Welsher, K.; Robinson, J.; Goodwin, A.; Zaric, S.; Dai, H. Nano-Graphene Oxide for Cellular Imaging and Drug Delivery. *Nano Res.* **2008**, *1*, 203–212.
28. Jung, J. H.; Jeon, J. H.; Sridhar, V.; Oh, I. K. Electroactive Graphene-Nafion Actuators. *Carbon* **2011**, *49*, 1279–1289.
29. Shin, K. Y.; Hong, J. Y.; Jang, J. S. Flexible and Transparent Graphene Films as Acoustic Actuator Electrodes Using Inkjet Printing. *Chem. Commun.* **2011**, *47*, 8527–8529.
30. Zhu, S. E.; Shabani, R.; Rho, J. H.; Kim, Y. S.; Hong, B. H.; Ahn, J. H.; Cho, H. J. Graphene-Based Bimorph Microactuators. *Nano Lett.* **2011**, *11*, 977–981.
31. Liu, J.; Wang, Z.; Zhao, Y.; Cheng, H.; Hu, C.; Jiang, L.; Qu, L. Three-Dimensional Graphene-Polypyrrole Hybrid Electrochemical Actuator. *Nanoscale* **2012**, *4*, 7563–7568.
32. Liu, J.; Wang, Z.; Xie, X.; Cheng, H.; Zhao, Y.; Qu, L. A Rationally-Designed Synergetic Polypyrrole/Graphene Bilayer Actuator. *J. Mater. Chem.* **2012**, *22*, 4015–4020.
33. Liang, J.; Huang, Y.; Oh, J.; Kozlov, M.; Sui, D.; Fang, S.; Baughman, R. H.; Ma, Y. F.; Chen, Y. Electromechanical Actuators Based on Graphene and Graphene/Fe_3O_4 Hybrid Paper. *Adv. Funct. Mater.* **2011**, *21*, 3778–3784.
34. Liang, J.; Xu, Y.; Huang, Y.; Zhang, L.; Wang, Y.; Ma, Y.; Li, F.; Guo, T.; Chen, Y. Infrared-Triggered Actuators from Graphene-Based Nanocomposites. *J. Phys. Chem. C* **2009**, *113*, 9921–9927.
35. Wu, C.; Feng, J.; Peng, L.; Ni, Y.; Liang, H.; He, L.; Xie, Y. Large-Area Graphene Realizing Ultrasensitive Photothermal Actuator with High Transparency: New Prototype Robotic Motions under Infrared-Light Stimuli. *J. Mater. Chem.* **2011**, *21*, 18584–18591.
36. Li, D.; Muller, M. B.; Gilje, S.; Kaner, R. B.; Wallace, G. G. Processable Aqueous Dispersions of Graphene Nanosheets. *Nat. Nanotechnol.* **2008**, *3*, 101–105.
37. Chen, H.; Müller, M. B.; Gilmore, K. J.; Wallace, G. G.; Li, D. Mechanically Strong, Electrically Conductive, and Biocompatible Graphene Paper. *Adv. Mater.* **2008**, *20*, 3557–3561.
38. Dikin, D. A.; Stankovich, S.; Zimney, E. J.; Piner, R. D.; Dommett, G. H. B.; Evmenenko, G.; Nguyen, S. T.; Ruoff, R. S. Preparation and Characterization of Graphene Oxide Paper. *Nature* **2007**, *448*, 457–460.
39. Nair, R. R.; Wu, H. A.; Jayaram, P. N.; Grigorieva, I. V.; Geim, A. K. Unimpeded Permeation of Water through Helium-Leak-Tight Graphene-Based Membranes. *Science* **2012**, *335*, 442–444.
40. Pei, S.; Zhao, J.; Du, J.; Ren, W.; Cheng, H.-M. Direct Reduction of Graphene Oxide Films into Highly Conductive and Flexible Graphene Films by Hydrohalic Acids. *Carbon* **2010**, *48*, 4466–4474.
41. Baughman, R. H.; Cui, C. X.; Zakhidov, A. A.; Iqbal, Z.; Barisci, J. N.; Spinks, G. M.; Wallace, G. G.; Mazzoldi, A.; de Rossi, D.; Rinzler, A. G.; *et al.* Carbon Nanotube Actuators. *Science* **1999**, *284*, 1340–1344.
42. Rogers, G. W.; Liu, J. Z. Graphene Actuators: Quantum-Mechanical and Electrostatic Double-Layer Effects. *J. Am. Chem. Soc.* **2011**, *133*, 10858–10863.
43. Lee, S. H.; Lee, D. H.; Lee, W. J.; Kim, S. O. Tailored Assembly of Carbon Nanotubes and Graphene. *Adv. Funct. Mater.* **2011**, *21*, 1338–1354.
44. Chen, J. H.; Jang, C.; Xiao, S.; Ishigami, M.; Fuhrer, M. S. Intrinsic and Extrinsic Performance Limits of Graphene Devices on SiO_2. *Nat. Nanotechnol.* **2008**, *3*, 206–209.
45. Li, X.; Zhu, Y.; Cai, W.; Borysiak, M.; Han, B.; Chen, D.; Piner, R. D.; Colombo, L.; Ruoff, R. S. Transfer of Large-Area Graphene Films for High-Performance Transparent Conductive. *Nano Lett.* **2009**, *9*, 4359–4363.

46. Mattevi, C.; Kim, H.; Chhowalla, M. A Review of Chemical Vapour Deposition of Graphene on Copper. *J. Mater. Chem.* **2011**, *21*, 3324–3334.
47. Kim, K. S.; Zhao, Y.; Jang, H.; Lee, S. Y.; Kim, J. M.; Kim, K. S.; Ahn, J. H.; Kim, P.; Choi, J. Y.; Hong, B. H. Large-Scale Pattern Growth of Graphene Films for Stretchable Transparent Electrodes. *Nature* **2009**, *457*, 706–710.
48. Park, S.; An, J.; Jung, I.; Piner, R. D.; An, S. J.; Li, X.; Velamakanni, A.; Ruoff, R. S. Colloidal Suspensions of Highly Reduced Graphene Oxide in a Wide Variety of Organic Solvents. *Nano Lett.* **2009**, *9*, 1593–1597.
49. Stankovich, S.; Dikin, D. A.; Piner, R. D.; Kohlhaas, K. A.; Kleinhammes, A.; Jia, Y.; Wu, Y.; Nguyen, S. T.; Ruoff, R. S. Synthesis of Graphene-Based Nanosheets *via* Chemical Reduction of Exfoliated Graphite Oxide. *Carbon* **2007**, *45*, 1558–1565.
50. Moon, I. K.; Lee, J. H.; Ruoff, R. S.; Lee, H. Y. Reduced Graphene Oxide by Chemical Graphitization. *Nat. Commun.* **2010**, *1*, 73.
51. Zhao, Y.; Wei, J.; Vajtai, R.; Ajayan, P. M.; Barrera, E. V. Iodine Doped Carbon Nanotube Cables Exceeding Specific Electrical Conductivity of Metals. *Sci. Rep.* **2011**, *1*, 83.
52. Jung, N.; Kim, N.; Jockusch, S.; Turro, N. J.; Kim, P.; Brus, L. Charge Transfer Chemical Doping of Few Layer Graphenes: Charge Distribution and Band Gap Formation. *Nano Lett.* **2009**, *9*, 4133–4137.
53. Rao, A. M.; Eklund, P. C.; Bandow, S.; Thess, A.; Smalley, R. E. Evidence for Charge Transfer in Doped Carbon Nanotube Bundles from Raman Scattering. *Nature* **1997**, *388*, 257–259.
54. Grigorian, L.; Williams, K. A.; Fang, S.; Sumanasekera, G. U.; Loper, A. L.; Dickey, E. C.; Pennycook, S. J.; Eklund, P. C. Reversible Intercalation of Charged Iodine Chains into Carbon Nanotube Ropes. *Phys. Rev. Lett.* **1998**, *80*, 5560–5563.
55. Hummers, W. S.; Offeman, R. E. Preparation of Graphitic Oxide. *J. Am. Chem. Soc.* **1958**, *80*, 1339–1339.
56. El-Kady, M. F.; Strong, V.; Dubin, S.; Kaner, R. B. Laser Scribing of High-Performance and Flexible Graphene-Based Electrochemical Capacitors. *Science* **2012**, *335*, 1326–1330.